Effects of negative shear on loads for a 15 MW offshore wind turbine during low-level jet events

Effects of negative shear on loads for a 15 MW offshore wind turbine during low-level jet events

Fahim Masud Ahmed[1], **Mostafa Bakhoday Paskyabi**[1]
[1]Geophysical institute, Allégaten 70, 5020 Bergen, Norway
E-mail: fahim.masud1999@hotmail.com

Abstract. Wind turbines are more often interacting with the negative shear region of a low-level jet due to increasing turbine sizes. However, the effects of negative shear on wind turbines are not sufficiently studied, particularly for offshore wind applications. In this paper, we studied the effects of negative shear on wind turbine loading. This was done using user-defined wind profiles and a model chain. The model chain consisted of a turbulence generator and a wake modelling tool coupled to an aero-hydro-servo-elastic engineering tool. We observed significant variations in the structural loading in the case of low-level jets. We also observed changes in the power spectral density estimates. Additionally, we briefly examined the wake recovery distance.

1. Introduction

Low-Level Jets (LLJs) are high speed air currents that occur in the Atmospheric Boundary Layer (ABL) [1]. They are characterized by a wind maximum at the top of the nocturnal inversion [2]. A wind maximum implies a negative shear region and a positive shear region above and below the maximum, respectively. Wind turbines have been designed with the expectation of facing positive shear, and there are not enough studies considering the effects of negative shear on wind turbines. This is becoming increasingly important as wind turbines grow larger, and more often interact with LLJ peaks [3]. This applies in particular to offshore wind turbines [4], since the growth of turbine dimensions are not limited by transportation [5]. However, there are some examples of studies considering the negative shear effects on wind turbines. A previous study [3] found that the negative shear region had positive effects on the mechanical loading.

The formation of LLJs may be attributed to different mechanisms depending on location. Above the Great Plains, the formation of LLJs are often attributed to Inertial Oscillations (IOs) [2, 6]. In coastal areas, the formation of LLJs are often attributed to baroclinic effects [6, 7]. LLJs above the Southern North Sea are attributed to both IOs and baroclinic effects [8]. In the IO mechanism [2], a temperature inversion leads to the decoupling of the surface from the wind, and the friction effects are reduced [1, 9]. An IO is induced due to the imbalance between the Coriolis force and the pressure-gradient forces [9]. The wind reaches supergeostrophic values later at night when the original daytime subgeostrophic wind is accelerated [1, 2, 9]. In the baroclinicity mechanism, a horizontal temperature gradient results in a sloped isobaric surface. Due to the thermal wind relationship, the geostrophic wind decreases with height. Furthermore, the actual wind is reduced near the surface due to friction. This results in the formation of LLJs [1, 9]. The temperature gradient can form from sloping terrain [9, 10], land-sea differential heating [9, 11] or cold fronts [9].

There are two methods for studying the effect of LLJs on wind turbines (i.e. load and wake characteristics). First option is to use data from measurements and the second option is to model synthetic LLJ events. The first option has the least uncertainty, but expensive equipment is needed. Therefore, the second option is usually preferred [3]. For the latter, turbulence simulators and wake modelling engineering tools are required. Wake modelling tools can be separated into low-, mid- and high-fidelity. Low-fidelity models are fast, but they fail to capture important wake characteristics. An additional limitation is that they don't account for the structural loading. In the high-fidelity models, results are accurate and the structural loading is accounted for. However, the models are computationally expensive. From an engineering perspective, this prevents high-fidelity models from being useful in the design process. Lately, mid-fidelity models have gained popularity. Mid-fidelity models, coupled with aero-elastic engineering tools, try to capture important characteristics while still being fast and relatively inexpensive [12].

The aim of this paper is to study the effects of a LLJ wind profile compared to a reference wind profile on structural loading during stable conditions. The jet height is at hub height, and the wind profiles are modelled equal below the hub height. This will be done using a model chain consisting of TurbSim [13], FAST.Farm [14] and OpenFAST [15]. OpenFAST is an engineering tool coupled to FAST.Farm, and it is responsible for the modelling of the aero-hydro-servo-elastic dynamics. FAST.Farm is a mid-fidelity wake modelling tool, and TurbSim is a turbulence simulator. We will use the IEA 15 MW Reference Wind Turbine (RWT) [16] with a semi-submersible floating platform [17]. The goal of this paper is to:

- understand how structural loading is affected in the presence of the negative shear of a LLJ.

Understanding the impact of LLJs on wind turbines is critical. There are concerns of higher generated moment on the turbine due to the wind shear. Additionally, there are concerns of an augmentation of fatigue loading in the presence of LLJs [18]. The impact of LLJs also extend to the wind turbine wake [19]. Therefore, we will also briefly look at the wake recovery distance.

From hereon, the paper is divided into the following sections. Section 2 describes the methodology used in this study. Section 3 presents and analyzes the results, and section 4 gives the conclusion of the study.

2. Method

The model chain used in this study consisted of TurbSim [13], FAST.Farm [14] and OpenFAST [15]. TurbSim was used to generate wind fields with a reference wind profile and a LLJ wind profile. The wind fields were used as inputs in FAST.Farm to simulate the wake and aero-hydro-servo-elastic dynamics. FAST.Farm uses OpenFAST to solve the latter [14].

2.1. TurbSim simulation setup

TurbSim produces a full-field flow containing coherent turbulent structures in three dimensions: y-axis, z-axis and t-axis. The turbulence is assumed to be stationary and Gaussian. Grid height and grid width were set to 550 m with 56 nodes in y- and z-directions. The analysis time was set to 1100 s with temporal resolution $\Delta t_t = 0.05$ s. Wind direction was set to 0°, which means that the wind inflow is perpendicular to the turbine. The wind profiles were user-defined and the wind spectra were defined by the IEC Kaimal model [13].

The LLJ profile in this study was made using two conditional representations. For $z > 150$ m, the following formulation was used [20]:

$$v_{LLJ}(z) = \left\{ v_{ref} + v_m \left[1 - \tanh^2 \left(C_s \frac{z - z_j}{z_j} \right) \right] \right\} \left(\frac{z}{z_{ref}} \right)^{p_0}, \tag{1}$$

where z is the height, v_{ref} is a reference velocity, v_m is the jet velocity, C_s is a shape parameter, z_j is the jet height, z_{ref} is the reference height and p_0 is the shear exponent. The formulation is based on the theory of plane wall jet [20]. The values used in equation (1) were: $v_{ref} = 10.7$ ms^{-1}, $v_m = 6.42$ ms^{-1}, $C_s = 0.8$, $z_j = 124$ m, $z_{ref} = 150$ m and $p_0 = 0.11$ [21]. For $z \leq 150$ m, the following neutral-atmosphere Power-Law (PL) equation was used [22]:

$$u(z) = u_{ref}\left(\frac{z}{z_{ref}}\right)^{p}, \tag{2}$$

where u_{ref} is the reference velocity, z is the height, z_{ref} is the reference height, p is the adjusted shear exponent for stable atmosphere. The adjusted shear exponent p was based on a paper by Newman and Klein [23], where they proposed a simplified equation for the shear exponent p as a function of a similarity function ϕ_m. The parametrization of the similarity function ϕ_m is dependent on the stability parameter ζ. By assuming a stable atmosphere and using similarity theory, the similarity function ϕ_m becomes: $\phi_m(\zeta) = 1 + 5\zeta$ [1, 23]. The resulting equation for the shear exponent p is shown below [23].

$$p(\phi_m) = p_0\phi_m(\zeta), \tag{3}$$

where $p_0 = 0.11$ [21] is the neutral atmosphere shear exponent and ϕ_m is the similarity function [23]. Adjusted shear exponent p was calculated by assuming $\zeta = 0.2$. The following values were used in equation (2): $u_{ref} = 16.94$ ms^{-1}, $z_{ref} = 150$ m and $p = 0.22$. The reference wind profile was calculated using the PL equation (see equation (2)) and the same set of values, but for all z.

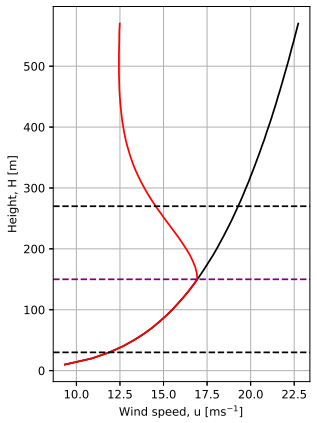

Figure 1. User-defined wind profiles used as inputs in TurbSim. LLJ profile (red) and reference profile (black).

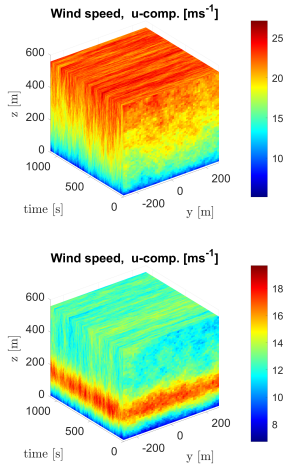

Figure 2. Three-dimensional wind fields simulated by TurbSim. Reference profile (upper) and LLJ profile (lower). Example from seed 1.

The surface roughness length z_0 was calculated using Charnock's relation [24], which gives z_0 above the ocean [1]:

$$z_0 = \alpha\frac{u_*^2}{g}, \tag{4}$$

Table 1. A summary of input parameters used in TurbSim. The values were rounded to three decimals.

Turb. model	IEC standard	Turb. intensity	Turb. type	z_0	c_1^u	c_1^v	c_1^w
IEC Kaimal	$61400-3$	5.0%	NTM	0.001	15.427	20.347	4.654

where α is the Charnock constant, u_* is the friction velocity, and $g = 9.81$ ms^{-2} is the gravitational acceleration. The friction velocity u_* was calculated based on the following empirical formulation [9]:

$$u_* = U_{10}\sqrt{C_d}, \tag{5}$$

where U_{10} is the mean wind velocity at 10 m and C_d is the drag coefficient. The following formulation for the drag coefficient was used [25]:

$$C_d = [a + bU_{10}] \times 10^{-3}, \tag{6}$$

where $a = 0.8$, $b = 0.065$, and both constants correspond to a Charnock constant $\alpha = 0.018$ [25]. U_{10} was 9.34 ms^{-1} for both wind profiles. Applying the values in equation (4) results in $z_0 = 0.0002$. For application in TurbSim, the variables were rounded to three decimals. However, this leads to $z_0 = 0$. Instead of this, we decided to round up to $z_0 = 0.001$.

The coherence was estimated using a simplified version of the following general coherence function [13]:

$$Coh_{i,j}^K = \exp\left(- a_K \left(\frac{r}{z_m} \right)^{\mathrm{CohExp}} \sqrt{\left(\frac{fr}{\bar{u}_m} \right)^2 + (b_K r)^2} \right). \tag{7}$$

This equation was simplified to the Davenport coherence model $\gamma_{i,j}^K$ by setting $\mathrm{CohExp} = b_K = 0$ [13]. For components $K = \{u, v, w\}$ between two points i and j, the Davenport coherence model $\gamma_{i,j}^K$ is given by the following equation [26]:

$$\gamma_{i,j}^K = \exp\left(- c_1^K \frac{fr}{\bar{u}_m} \right), \tag{8}$$

where c_1^K is the decay coefficient for components K, f is the frequency, r is the distance between points i and j, and $\bar{u}_m$ is the mean wind speed between points i and j. The decay coefficient c_1^K was calculated with the following model from Cheynet et al. [27]. The model is based on the stability parameter $\zeta = z/L$, and the authors concluded that the model is accurate for $-2 < \zeta < 0.2$ for the FINO1 site.

$$c_1^u = 11 + 1.8\exp(4.5\zeta), \tag{9}$$

$$c_1^v = 7.1 + 3.4\exp(6.8\zeta), \tag{10}$$

$$c_1^w = 3.5 + 0.7\exp(2.5\zeta). \tag{11}$$

The Monin-Obukhov length L (and by extension ζ) is positive in a stably stratified atmosphere [1], and therefore we assumed $\zeta = 0.2$.

2.2. Wind turbine model

The IEA 15 MW RWT was used throughout the study [16], and the University of Maine VolturnUS-S reference floating platform was used as the supporting structure [17]. The hub height of the turbine is 150 m and the rotor diameter D is 240 m. The mass of the total system is 20093 tonnes with a draft of 20 m. The structure is held in place by three catenary mooring lines [17]. The three blade passing frequencies at maximum rotor speed: 1P, 2P and 3P are 0.126 Hz, 0.252 Hz and 0.378 Hz, respectively [16].

*2.3. FAST.Farm v*3.2.1 *simulation setup*

FAST.Farm is a mid-fidelity engineering tool used to simulate the wake effects for wind turbines. The main FAST.Farm driver acts as a glue code for several modules. The wake effects are calculated based on principles of the Dynamic Wake Meandering (DWM) model with improvements [14]. The DWM model is based on works by Ainslie [28] and Larsen [29]. Ainslie described a numerical model to calculate the wake flow field based on the Navier-Stokes equations using a thin-shear layer approximation. The wake meandering model was described by Larsen and it is estimated using a system of differential equations. Improvements were made to the DWM implementation to better represent the wake. The improvements allow FAST.Farm to skew the wake centerline based on the inflow angle, account for wake acceleration, change the wake deficit evolution, calculate vertical and lateral wake meandering, and form an elliptical wake shape [14].

The domain properties are specified in the primary FAST.Farm input file. A low resolution domain extends across the flow field and a high resolution domain is placed around the turbine. The low resolution domain consisted of $Nx_{Low} = 601$, $Ny_{Low} = 45$ and $Nz_{Low} = 37$ spatial nodes. Grid resolution was $\Delta x_{Low} = 12$ m, $\Delta y_{Low} = 12$ m and $\Delta z_{Low} = 15$ m. The turbine was placed at $x = y = 0$ inside the high-resolution domain consisting of $Nx_{High} = 125$, $Ny_{High} = 50$, and $Nz_{High} = 54$ spatial nodes. The grid resolution was $\Delta x_{High} = 10$ m, $\Delta y_{High} = 10$ m and $\Delta z_{High} = 10$ m. The temporal resolutions were $\Delta t_{Low} = 1.0$ s and $\Delta t_{High} = 0.1$ s. Additionally, the time step $\Delta t = 0.010$ s and the water depth $D_w = 200$ m were specified in the primary OpenFAST input file for the modelling of wind turbine dynamics.

The aero-hydro-servo-elastic dynamics are handled by the OpenFAST module in FAST.Farm. It contains submodules to account for the different forces acting on the structure. AeroDyn calculates the aerodynamic loading based on the actuator line model and Blade-Element Momentum (BEM) theory, ElastoDyn is responsible for the structural dynamics, HydroDyn is responsible for the hydrodynamics and generates irregular waves based on the JONSWAP spectrum, and InflowWind is responsible for the wind inflow. The JONSWAP spectrum is calculated with the significant wave height H_s and peak spectral period T_p [15]. Inputs were based on a formulation by Carter [30], and were given by $H_s = 0.0248|U_{10}|^2$ and $T_p = 0.729|U_{10}|$. Substituting the mean wind velocity at 10 m for both profiles (i.e. $U_{10} = 9.34$ ms^{-1}) into the equations results in $H_s = 2.16$ m and $T_p = 6.81$ s. The wave conditions were kept constant across the simulations, and the effects were not studied. Taylor's frozen turbulence hypothesis is used by InflowWind to obtain local wind speeds from the TurbSim generated inflow file [13].

3. Results & discussion

A model chain consisting of TurbSim, FAST.Farm and OpenFAST was used to study the structural loading and wake recovery distance. Two wind profiles were used for the study: a reference profile and a LLJ profile. The results were averaged over six simulations for each wind profile type, and each simulation was run for 1100 s. First 200 s were dropped from the time series to account for model spin-up time for the load study. We used the following quantities for the load study: tower base streamwise shear force (TwrBsFxt), tower base spanwise shear force (TwrBsFyt), tower base side-to-side moment (TwrBsMxt), tower base

fore-aft moment (TwrBsMyt), yaw bearing roll moment (YawBrMxn), yaw bearing pitching moment (YawBrMyn), blade root out-of-plane shear force for blade 1 (RootFxc1) and blade root out-of-plane moment for blade 1 (RootMyc1). To study the mean wake recovery distance, an averaged wake was constructed from instantaneous wake data. 1100 s of instantaneous wake data was available. However, the first 300 s were dropped to ensure a fully developed wake before averaging.

Throughout this section, the standard deviation was used as a measure to compare and analyze the load quantities. The skewness and kurtosis for all time series involved were calculated, and they suggested Gaussian distributions for all variables (i.e. skewness of 0 and kurtosis of 3).

3.1. Wind field

The mean wind velocity at hub height was 16.94 ms^{-1} for both wind profiles. The standard deviations were 0.91 ms^{-1} and 0.66 ms^{-1} for the PL profile and the LLJ profile, respectively. This resulted in $TI_{PL} = 5.4\%$ and $TI_{LLJ} = 3.9\%$ at hub height. Across the rotor swept area, the average TI was 5.7% for the reference profile and 4.4% for the LLJ profile. Although both profiles were set in stable conditions, the atmosphere in the reference case was modelled slightly less stable, as a very low turbulence level is expected in the case of a LLJ event [31].

At the bottom of the rotor swept area (at 30 m), the mean wind velocity was $u_{30} = 11.89$ ms^{-1} for both wind profiles. This resulted in an average wind shear of 0.042 s^{-1} from hub height to the bottom of the rotor swept area. Above the hub height, the wind shear across the rotor swept area was 0.02 s^{-1} for the reference profile and -0.02 s^{-1} for the LLJ profile.

When modelling turbulence in TurbSim, the standard deviation for the wind velocity is assumed similar across all grid points [13]. For a LLJ profile, the turbulence is expected to decrease with height, even with lower wind speeds above the LLJ. This is because the standard deviation decreases as a result of the stably stratified atmosphere where LLJs are formed [31]. Due to the modelling approach used in TurbSim, this was not properly represented, and the TI increased above jet height in our wind model. Even though this effect is unexpected, and is one of the limitations of TurbSim, it is not unphysical. Schepers et al. [31] observed an increase in TI above jet height, but the authors remarked that this observation was hard to explain.

Another limitation was the consideration of stability in TurbSim. Throughout the study, we considered a stably stratified atmosphere and calculated the input parameters for TurbSim accordingly. However, when using the IEC Kaimal model, the atmosphere is automatically considered neutral by TurbSim [13]. This means that the Richardson number Ri, which is the relationship between buoyancy and shear forces [1], was automatically set to zero, and the buoyancy forces were not considered.

3.2. Structural dynamics

To account for the dynamic nature of wind forcing, the Damage Equivalent Load (DEL) was calculated. DEL considers both the amplitude of the time series and the amount of oscillations, and returns the load range that will inflict the same amount of damage in N amount of cycles as the actual loading. It is calculated by using the Rainflow cycle-counting algorithm and the Wöhler exponent of the material. The DEL is given by the following equation [32, 33]:

$$DEL = \left(\frac{\sum_i (R_i^m n_i)}{n_{eq}} \right)^{\frac{1}{m}}, \tag{12}$$

where R_i is the amplitude of the time series, n_i is the number of cycles, $n_{eq} = 900$ is the number of cycles to equivalent damage and m is the Wöhler exponent of the material. The Wöhler exponent m was set to 3 for the steel tower and 10 for composites blades [32, 33].

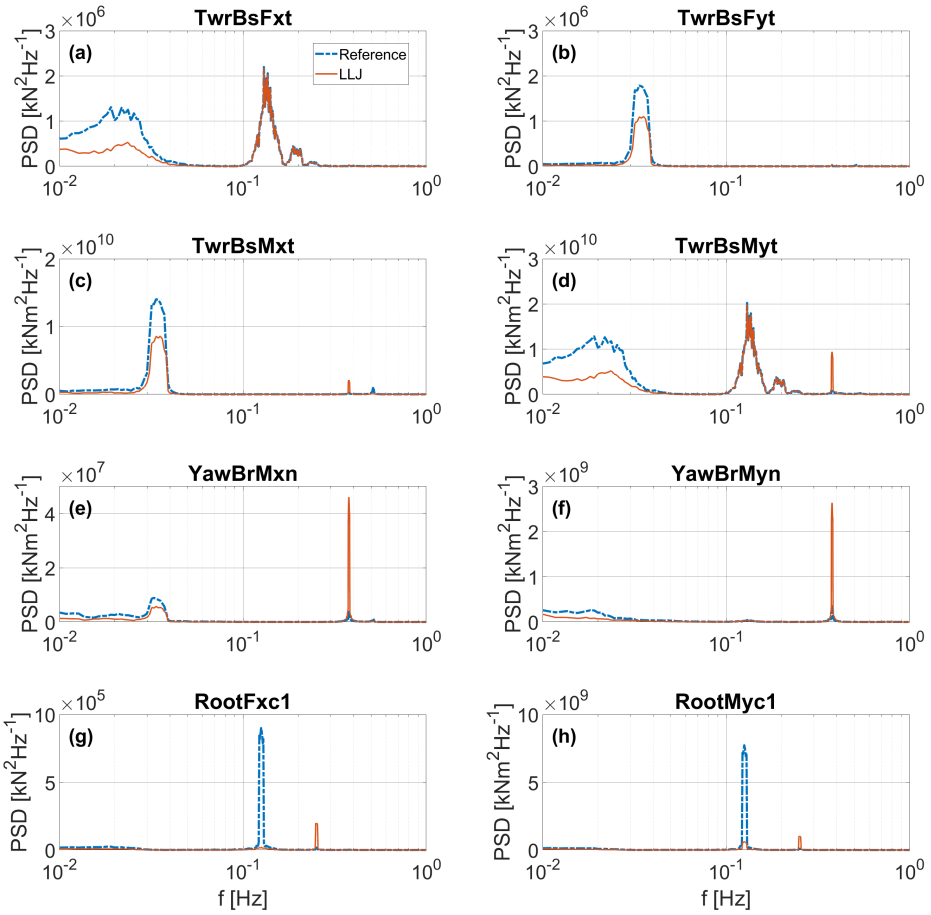

Figure 3. Power Spectral Density (PSD) estimates for the given load quantities displayed in semi-logarithmic plots. Generally, lower energy levels were observed for the LLJ case.

Table 2. DEL for load parameters and their change in the case of a LLJ event.

Parameter	DEL_{ref}	DEL_{LLJ}	Change
TwrBsFxt [kN]	506.3	476.1	−6.0%
TwrBsFyt [kN]	184.1	142.0	−22.9%
TwrBsMxt [kNm]	18289.3	15670.7	−14.3%
TwrBsMyt [kNm]	48836.8	48762.5	−0.2%
YawBrMxn [kNm]	944.1	1420.6	+50.5%
YawBrMyn [kNm]	6996.8	10745.3	+53.6%
RootFxc1 [kN]	285.5	178.1	−37.6%
RootMyc1 [kNm]	22588.3	13493.3	−40.3%

3.2.1. Tower base forces and moments. A decrease in DEL was observed for the tower base shear forces in both streamwise (TwrBsFxt) and spanwise directions (TwrBsFyt) (see Table 2). This is consistent with findings by Gutierrez et al. [3], where the authors found a reduction in the standard deviation proportional to the amount of negative shear inside the rotor swept area. The Power Spectral Density (PSD) estimate for TwrBsFxt in Figure 3a shows peaks at the platform pitch motion frequency (i.e. at 0.02 Hz) and the frequency of 1P. However, the contribution from the platform pitch motion was decreased in the LLJ case. From the PSD estimate for TwrBsFyt in Figure 3b, it was also observed that the main contribution was from the platform roll motion (i.e. at 0.03 Hz). The response at the platform roll motion frequency was decreased in the LLJ case.

From Table 2, it was observed a decrease in DEL for the TwrBsMxt. This is consistent with findings by Gutierrez et al. [3], where the authors found a decrease in oscillations in the plane of rotation in the case of negative shear. From the PSD estimate for TwrBsMxt in Figure 3c, we observed less contribution from platform roll motion (at 0.03 Hz) in the LLJ case. However, the peak at the frequency of 3P was relatively large. This suggests that a larger response in the TwrBsMxt at the frequency of 3P might occur in the case of a LLJ.

The smallest change in DEL was observed for TwrBsMyt (see Table 2). This result was expected as the TwrBsMyt is largely dependent on the thrust and tower height [34]. Since the thrust forces were similar, the TwrBsMyt was also expected to be similar. From the PSD estimate for TwrBsMyt in Figure 3d, peaks were observed at around 0.2 Hz, 0.13 Hz and 0.38 Hz. The first peak at 0.2 Hz was the contribution of the platform pitch motion, and this was observed for both cases. Although, the peak was at a higher value for the reference case. This was likely due to a lower standard deviation for platform pitch motion in the LLJ case, which was most likely due to lower turbulence levels. The second peak at 0.13 Hz corresponded roughly to the frequency of 1P. It was the peak containing the most energy, thus showing its considerable effect on the TwrBsMyt independent of the wind profile. The last peak at 0.38 Hz corresponded to the frequency of 3P. Even though it was present in the reference case, the peak was at a relatively low value compared to the LLJ case. This suggests that a larger response in the TwrBsMyt at the frequency of 3P might be expected in the case of a LLJ.

3.2.2. Yaw bearing moments. An increase in DEL was observed for the YawBrMxn and YawBrMyn in Table 2. This was most likely caused by the negative shear above the hub height. This is supported by additional simulations (not shown here), where we observed an increase in yaw bearing moments in the case of larger negative wind gradient above the hub height.

PSD estimate of YawBrMxn in Figure 3e shows peaks at 0.03 Hz and the frequency of 3P. For the reference case, the largest contribution was observed from the platform roll motion (at 0.03 Hz). For the LLJ case, the platform roll motion revealed a smaller impact on YawBrMxn than in the reference case. However, we observed a much larger peak at the frequency of 3P for the LLJ case. This suggests that a larger response in the TwrBsMxt at the frequency of 3P might occur in the case of negative shear inside the rotor swept area.

PSD estimate of YawBrMyn in Figure 3f shows a concentrated narrow peak around the frequency of 3P. This was different from the reference case, where we observed peaks around 0.005 Hz and the frequency of 3P. However, the latter peak was at a much lower value for the reference case compared to the LLJ case. The first peak at 0.005 Hz denoted the contribution from the platform sway motion. The peak at 0.005 Hz was not present for the LLJ case, suggesting that the sway motion had less effect during the LLJ. The platform pitch motion had little contribution, and this was consistent with findings by Myrtvedt et al. [34].

3.2.3. Blade root out-of-plane force and moment for blade 1. We observed a decrease in DEL (see Table 2) for RootFxc1 due to the lower turbulence levels in the LLJ case (with narrow peak

at around the frequency of 1P, see Figure 3g). The peak at the frequency of 1P was lower for the LLJ case. However, there was a larger peak at the frequency of 2P. This suggests that a larger response in the RootFxc1 at the frequency of 2P might occur during a LLJ event.

From Table 2, we observed a large decrease in DEL for RootMyc1. The decrease in the standard deviation of RootMyc1 was roughly equal to the decrease in the standard deviation of out-of-plane tip deflection for blade 1 (OoPDefl1). The cause of the lower standard deviation for OoPDefl1 was likely the lower turbulence levels, causing decrease in the blade root moment. Schepers et al. [31] remarked that the blade flapwise moments were decreased in the presence of a LLJ, and they attributed this decrease to the low turbulence intensity. However, Gutierrez et al. [3] argued that the negative shear had minimal effects on the blade loads, and it slightly reduces the streamwise bending moment. A combination of previous findings, and the results from this paper, suggested that the decrease in DEL for RootMyc1 was mostly due to the lower turbulence level, and that the negative shear had less impact. However, it was difficult to precisely attribute one mechanism to the decrease in DEL. Furthermore, the decrease in DEL was substantial compared to the relatively small difference in TI between the wind profiles. Therefore, further work is recommended.

It was observed from the PSD estimate for RootMyc1 in Figure 3h that the largest peak was at the frequency of 1P in the reference case. This was different from the LLJ case, where the largest peak was at the frequency of 2P, and the peak at the frequency of 1P was relatively low. This suggests that a larger response in the RootMyc1 at the frequency of 2P might occur during a LLJ event.

3.3. Wake recovery

The mean wake recovery distance at $y = 0$ was estimated using the RMSE. It was calculated at streamwise distance $x_i = i\Delta x_{Low}$ for $i = 1, 2, 3, ..., Nx_{Low}$. We considered the wake to be recovered at distance x_i when the RMSE was 0.5 or lower for the first time. Following this criteria, the wake recovered at 10.25D for the reference case and 13D for the LLJ case, respectively. The wake recovery distance was larger for the LLJ profile likely due to the lower levels of turbulence [35]. Even for the reference case, the wake recovery distance was large due to the stable atmosphere assumption [36].

4. Conclusion

In this paper, we studied the effects of a low-level jet profile compared to a reference power-law profile. The wind profiles below hub height were kept roughly equal, and only the effects of negative shear above the hub height were considered. The model chain used in this study consisted of a turbulence generator (TurbSim) and a wake modelling tool (FAST.Farm) coupled to an aero-hydro-servo-elastic engineering tool (OpenFAST). The latter handles the wind turbine dynamics, and provides the results for the load quantities.

Generally, the negative shear of low-level jets had a positive effect on the loading. We observed a decrease in the damage equivalent load for the majority of load parameters. This was partly due to the lower turbulence levels associated with low-level jets, and partly due to the negative wind shear effect. Exceptions to this were the yaw bearing moments in both streamwise and spanwise directions, where we observed an increase likely due to the negative shear. Tower base fore-aft moment stayed roughly equal. We also observed that the frequency of 2P and 3P had larger peaks in the power spectral density estimates for the load quantities during low-level jets.

In addition to the load quantities, we briefly studied the mean wake recovery distance. This was done by calculating the Root-Mean-Square-Error (RMSE) at each streamwise distance with 0.5D interval. The results showed an increase in wake recovery distance in the case of a LLJ event, likely due to the lower turbulence levels.

Acknowledgments
The authors would like to thank Etienne Cheynet (UiB), Bruno Antonio Roccia (UiB) and Marte Godvik (Equinor) for their support and insight. This work was supported by the CONWIND-project of the Research Council of Norway with grant number of UB101292101.

References
[1] Stull R B 1988 *An Introduction to Boundary Layer Meteorology* 1st ed (Dordrecht, The Netherlands: Kluwer Academic Publishers)
[2] Blackadar A K 1957 *Bulletin of the American Meteorological Society* **38** 283–290
[3] Gutierrez W, Ruiz-Columbie A, Tutkun M and Castillo L 2017 *Wind Energy Science* **2** 533–545
[4] Aird J A, Barthelmie R J, Shepherd T J and Pryor S C 2022 *Energies* **15**
[5] Breton S P and Moe G 2009 *Renewable Energy* **34** 646–654
[6] Pichugina Y L, Brewer W A, Banta R M, Choukulkar A, Clack C T M, Marquis M C, McCarty B J, Weickmann A M, Sandberg S P, Marchbanks R D and Hardesty R M 2017 *Wind Energy* **20** 943–1127
[7] Jiang Q, Wang S and O'Neill L 2010 *Monthly Weather Review* **138** 3185–3187, 3189–3206
[8] Wagner D, Steinfeld G, Witha B, Wurps H and Reuder J 2019 *Meteorologische Zeitschrift* **28** 389–415
[9] Paskyabi M B, Bui H and Penchah M M 2022 *HIPERWIND project* 131
[10] Holton J R 1967 *Tellus A: Dynamic Meteorology and Oceanography* **19** 199
[11] Burk S D and Thompson W T 1996 *Monthly Weather Review* **124** 668–686 ISSN 00270644
[12] Wise A S and Bachynski E E 2020 *Wind Energy* **23** 1266–1285
[13] Jonkman B J 2014 TurbSim User's Guide v2.00.00 Tech. rep. National Renewable Energy Laboratory (NREL) Golden, Colorado
[14] Jonkman J and Shaler K 2021 FAST.Farm User's Guide and Theory Manual Tech. rep. NREL
[15] National Renewable Energy Laboratory 2022 OpenFAST Documentation — OpenFAST v3.2.1 documentation URL `https://openfast.readthedocs.io/en/main/`
[16] Gaertner E, Rinker J, Sethuraman L, Anderson B, Zahle F and Barter G 2020 IEA Wind TCP Task 37: Definition of the IEA 15 MW Offshore Reference Wind Turbine Tech. rep. International Energy Agency Paris, France
[17] Allen C, Viselli A, Dagher H, Goupee A, Gaertner E, Abbas N, Hall M and Barter G 2020 Definition of the UMaine VolturnUS-S Reference Platform Developed for the IEA Wind 15-Megawatt Offshore Reference Wind Turbine Tech. rep. National Renewable Energy Laboratory Golden, Colorado
[18] Gutierrez W, Araya G, Basu S, Ruiz-Columbie A and Castillo L 2014 *Journal of Physics: Conference Series* vol 524
[19] Bhaganagar K and Debnath M 2014 *Energies* **7** 5740–5763
[20] Zhang X, Yang C and Li S 2019 *Engineering Applications of Computational Fluid Mechanics* **13** 300–308
[21] Hsu S A, Meindl E A and Gilhousen D B 1994 *Journal of Applied Meteorology* **33** 757–765
[22] Frost R 1948 *Quarterly Journal of the Royal Meteorological Society* **74** 316–338
[23] Newman J F and Klein P M 2014 *Resources* **3** 81–105
[24] Charnock H 1955 *Quarterly Journal of the Royal Meteorological Society* **81** 639–640
[25] Paskyabi M B, Flügge M, Edson J B and Reuder J 2013 *Energy Procedia* **35** 102–112
[26] Davenport A G 1962 *Proceedings of the Institution of Civil Engineers* **23**(3) 389–408
[27] Cheynet E, Jakobsen J B and Reuder J 2018 *Boundary-Layer Meteorology* **169** 429–460
[28] Ainslie J F 1988 *Journal of Wind Engineering and Industrial Aerodynamics* **27** 213–224
[29] Larsen G C, Madsen H A, Thomsen K and Larsen T J 2008 *Wind Energy* **11** 377–395
[30] Carter D J 1982 *Ocean Engineering* **9** 17–33
[31] Schepers G, Van Dorp P, Verzijlbergh R, Baas P and Jonker H 2021 *Wind Energy Science* **6** 983–996
[32] Nybø A, Nielsen F G and Godvik M 2021 *Wind Energy* 1482–1500
[33] International Electrotechnical Commission 2015 IEC TS 61400-13: Wind Turbines - Part 13: Measurement of mechanical loads Tech. rep. IEC Paris, France
[34] Myrtvedt M H, Nybø A and Nielsen F G 2020 *J. Phys.: Conf. Series* vol 1669
[35] Gutierrez W, Ruiz-Columbie A, Tutkun M and Castillo L 2019 *Renewable and Sustainable Energy Reviews* **108** 380–391
[36] Cañadillas B, Foreman R, Barth V, Siedersleben S, Lampert A, Platis A, Djath B, Schulz-Stellenfleth J, Bange J, Emeis S and Neumann T 2020 *Wind Energy* **23** 1249–1265